Cracks starting from Hertzian contact with friction

W. Endres[1] and **J. Coutlakis**[2]
(First received February 1993; Final version July 1993)

Abstract

Cracks due to repeated contact stresses are found in pitting of gear teeth and in T-heads which are used to attach blades in turbomachinery. In these two examples the directions of the cracks are very different and an explanation was sought. In gears, both the normal and the tangential loads are repeating, whilst in T-heads the normal load is steady, but the tangential friction load is repeating. Crack growth theories were applied which allowed calculation of the direction of the crack path. Good agreement was found with the observed initial directions of cracks in gears leading to pitting, as well as those cracks in T-heads. The crack directions varied strongly with the coefficient of friction in gears, whilst in the case of T-heads the crack direction was the same for all values of the coefficient of friction. Size effects make larger contact areas more susceptible to failure and require lower allowable pressures. This is an important conclusion. The coefficient of friction was the governing parameter in all cases and it should be kept as low as possible.

Nomenclature

b	half the contact width
E	Young's modulus
f	coefficient of friction
F	load
K_1	stress intensity factor, opening mode due to tensile stress
K_{11}	stress intensity factor, sliding mode due to shear stress
p	pressure
p_0	maximum Hertzian pressure
r	radius
S	strain energy density factor
SIF	stress intensity factor
x, y	dimensionless cartesian coordinates
z	complex variable $z = x + iy$
σ	normal stress
τ	shear stress
ν	Poisson's ratio

[1]Professor, Department of Mechanical Engineering, University of Stellenbosch, Stellenbosch, 7600 Republic of South Africa

[2]M.Eng (Mechanical) student, presently with Creative Engineering, Stellenbosch

Introduction

Contact forces of compression and shear are classical engineering problems in railways and gears. Failure records in America of government and commercial equipment show that sliding and rolling elements under heavy loads are among the most unreliable mechanical components.

Rolling contact phenomena are of considerable practical and theoretical importance, since the region of the contact zone between machine elements moving in rolling contact, or in combined rolling and sliding, is subject to stresses and deformations that are not easy to duplicate in other types of equipment.

An extensive literature exists, some of which was reviewed in [1], and research is continuing as loads and speeds continue to increase. The understanding of the failure mechanism still leaves some open questions, particularly for pitting in gears where numerous explanations and theories have been proposed.

Pitting is a surface fatigue failure and occurs where surfaces come into contact under conditions of rolling/sliding motion, high surface loading, and marginal lubrication. It starts at small asperities and becomes wider as it grows (Figure 1a). The pitting cracks start at angles of 10 to 30°. The coefficient of friction in gears is normally smaller than 0.15.

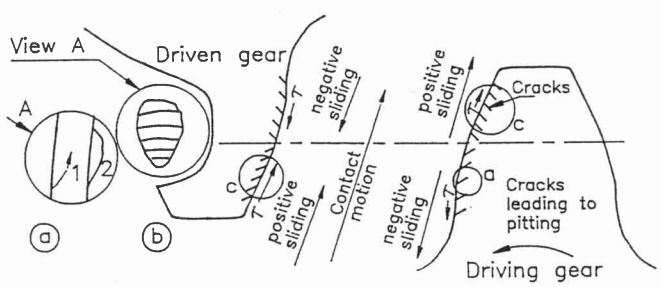

Figure 1. (a) Pitting crack growing (1) and fully developed (2), (b) pitting crack orientations in gear teeth, from [5]. For details compare Figure 12.

One established explanation, the hydraulic pressure mechanism, was initiated by Way in 1935. Way concluded from experiments under pure rolling that a lubricant is necessary for pitting, that the fluid enters the crack and is trapped as the contact area closes the crack. The pressure then increases and tensile stresses in the crack tip cause

the crack to grow.[2;3] Kaneta [4] investigated a three-dimensional crack inclined at 45° against the surface with oil present in the crack and discussed crack growth under shear (mode II) and tension (mode I).

These theories serve well as an explanation for cracks and pitting formed in the dedenda of gear teeth (Figure 1b, redrawn from Dudley [5] and Niemann [6]). However they fail to explain the normally less severe cracking in the addenda regions, where the lubricant gets squeezed out of the crack and is not trapped. They also do not deal with the start of the crack.

The authors therefore doubt that the hydraulic pressure mechanism plays any role in crack initiation. Further, after initiation, other mechanisms must exist to propagate cracks in the addenda and consequently in the dedenda as well.

An important observation in Figure 1b is that there is an obvious relationship between the direction of the shear stress applied to the surface and the direction of the cracks. Figure 2 represents a close-up of the contact area (in the addendum) with two possible cracks and shows that a crack on the left side of the inclined load will be opened by tension, whilst the crack at the right side is mainly subject to shear. The orientation of the left crack in Figure 2 corresponds to pitting in the addenda of Figure 1b, detail c.

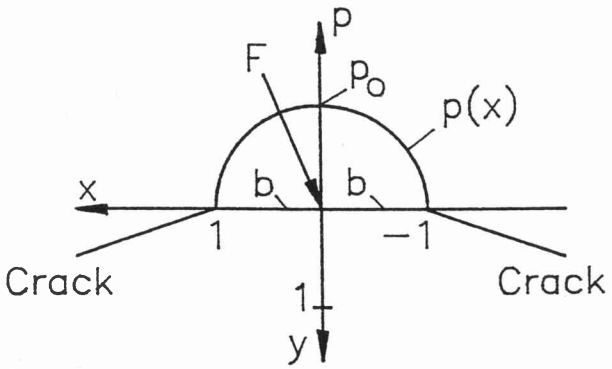

Figure 2. Inclined load F elliptically distributed tends to open the left crack by tension, whilst the right crack is mainly subject to shear. Vertical component of the pressure on the half space $y > 0$ is $p(x)$, the maximum value is p_0.

This idea was first proposed by Käser [7] and independently by Arcan [8] and was first used as a guideline for this study.

Other applications where fatigue cracks and fretting near the edge of contact areas have caused problems include wedges in axial dovetails in generator rotors, as investigated by King & Lindley, [9] and recently in T-heads, where the normal load in the contact is steady, but the tangential friction load is repeating (Figure 3a). Note: Figure 3a shows only the right half of the geometry, which is symmetrical with respect to the centre line on the left of Figure 3a.

In both applications the final fatigue cracks start close to the edge of the contact area and run more or less perpendicular to the surface (Figure 3a). However, in the contact zone a thin surface layer is plastically deformed by shear, sometimes producing a step at the edge of the contact zone. Numerous very small randomly inclined cracks start in this layer. The final, almost perpendicular fatigue crack, shows no plastic deformation and starts from one of these small cracks (Figure 3b).

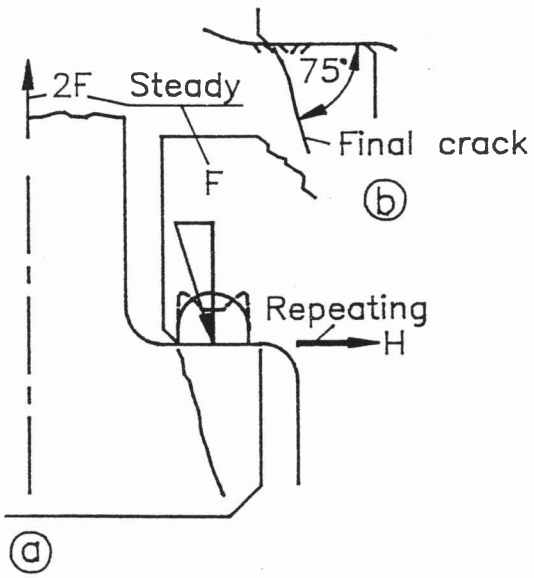

Figure 3. (a) Crack in T-head contact area (only right half shown) under steady vertical load F and repeating horizontal load H, (b) enlarged contact area.

In gears such plastic surface deformation by rolling and sliding is also observed (Figure 12), particularly if the surfaces are not very hard.

The aim of this investigation was to obtain a clearer understanding of the mechanism of the final fatigue cracks and the direction in which they start. The investigation concentrated on the left side of the contact zones in Figures 2 and 3 and considered only short cracks with a length a of 0.1 to 0.5 × b, where $2b$ is the width of contact zone.

Photoelastic investigation

Prior to the theoretical approach, described below, photoelastic tests were carried out.[1;10] These tests depend highly on the finish and the accuracy of the surfaces, as under most conditions the contact width $2b$ is narrow and asperities lead to local disturbances. Figure 4a shows a photoelastic test by Maul [10] of a cylinder pressed against a flat plate with a contact area which was 22.5 mm wide. At the left edge of the contact area a semicircular groove

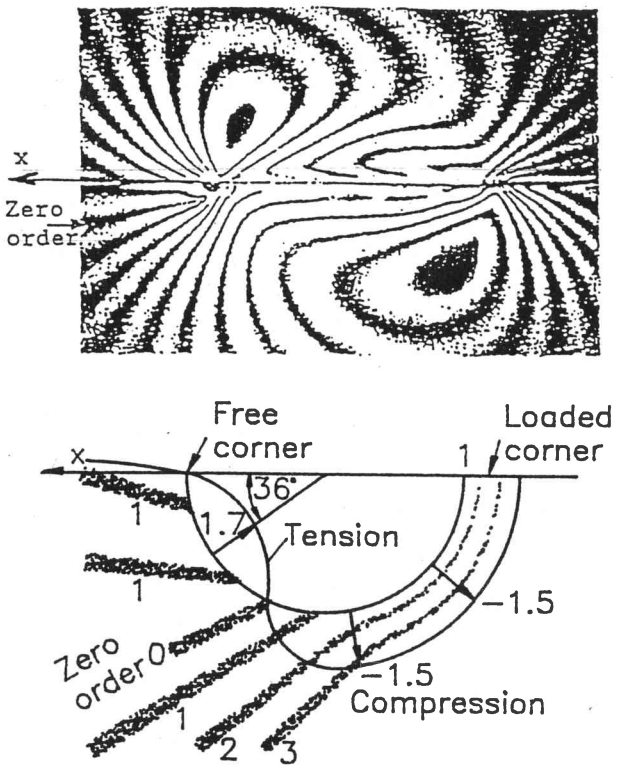

Figure 4. (a) Photoelastic test of a cylinder pressed against a flat plate, coefficient of friction $f = 0.2$ from [8], (b) enlarged semicircular notch at left side of contact area showing tensile stress along surface.

(radius $r = 0.75$ mm) was cut to aid in the observation of the stresses in the area where cracks were suspected to start.

The ratio of the tangential load to the vertical load was 0.2. On the left side of the groove, at an angle of approximately 36°, a tensile stress of approximately $0.055p_0$ was measured, which is a fourth of the value of the tensile peak ($\sigma_x = 0.4p_0$ at $x = 1$, see Figure 5) without the groove. Clearly the small round groove reduces the peak stress very effectively. This would not be the case if the groove were replaced by a small crack in a direction normal to the observed tensile stress, which roughly coincides with the direction of cracks in gears. It would be instructive to carry out photoelastic tests with such cracks in the future.

In the meantime, it was decided to examine different theoretical methods which could possibly describe the observed cracks.

The theoretical stress field

The stress field in gear tooth contacts was approximated by the plane-strain Hertzian equations. Local asperity peaks, which were not considered here, lead to local three-dimensional deviations from the plane-strain field. In T-heads with well-rounded contact corners, the Hertzian equations can also be used next to the edge as an approximation; compare the pressure distribution according to the dotted line and the elliptic one in Figure 3. Most real pressure distributions will fall between these two. The main difference is their slope at the edge of the contact. Therefore the theoretical investigations described below are limited to the Hertzian case of plane strain and start from closed solutions of the stress field as given by Föppl [11] or Smith & Liu.[12]

For a cylinder in contact with a semi-infinite plane, the stresses due to the normal load with the elliptic distribution

$$p = p_0 \times \sqrt{1 - x^2} \quad \text{(NB. } x \text{ normalized to } b = 1 \text{ at the edge of the contact)} \tag{1}$$

are given by Föppl [11] after the substitution

$$z = \cosh\gamma \text{ with } x + iy,\ \gamma = \alpha + i\beta \tag{2}$$

in the form

$$\begin{aligned} \sigma_{x_1} &= -p_0 \sin\beta \left[e^{-\alpha} - \sinh\alpha \tfrac{1-\sinh 2\alpha}{(\cosh 2\alpha - \cos 2\beta)} \right] \\ \sigma_{y_1} &= -p_0 \sin\beta \left[e^{-\alpha} + \sinh\alpha \tfrac{1-\sinh 2\alpha}{(\cosh 2\alpha - \cos 2\beta)} \right] \\ \tau_{x_{y_1}} &= \tfrac{-p_0 \sinh\alpha \sin\beta}{\cosh 2\alpha - \cos 2\beta} \end{aligned} \tag{3}$$

A tangential load fp caused by friction acting in the direction shown in Figure 2 leads to stresses

$$\begin{aligned} \sigma_{x_2} &= 2fp_0 \cos\beta e^{-\alpha} + f\tau_{x_{y_1}} \\ \sigma_{y_2} &= -f\tau_{x_{y_1}} \\ \tau_{x_{y_2}} &= -f\sigma_{x_1} \end{aligned} \tag{4}$$

For plane strain and the same materials, the contact width $2b$ is given by

$$2b = 2p_0 r \frac{(1-\nu^2)}{E} \tag{5}$$

with ν for Poisson's ratio and the radius r of the cylinder. Note: For two cylinders in contact r is replaced by

$$\frac{1}{\frac{1}{r_1} + \frac{1}{r_2}}$$

The normal force becomes

$$p = \pi p_0 \frac{b}{2} \tag{6}$$

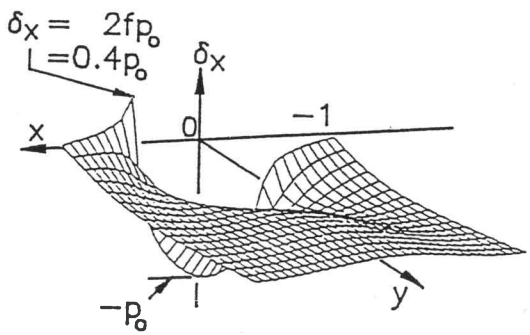

Figure 5. Tensile stress σ_x in Hertzian contact with shear $f = 0.2$.

The distribution of the tensile stress σ_x is shown in Figure 5 for a coefficient of friction of $f = 0.2$. At the left end of the contact zone the tensile stress parallel to the surface has a peak of $2fp_0$, where p_0 is the maximum Hertzian pressure. In gears with p_0 often greater than 1 500 MPa and $f = 0.15$ (which is a high value assuming marginal lubrication) the tensile peak is greater than 450 MPa, which is close to the endurance limit.

Crack path calculation

Fatigue crack propagation in a highly nonlinear stress field is certainly difficult to predict. The theoretical investigations described below are limited to the case of plane strain and start from the previously mentioned closed solutions of the stress field. They assume, in accordance with St Venant's principle, that at some distance roughly equal to the crack length the presence of the crack does not alter the stress field. Thus the stress field of the uncracked geometry can be used to predict the direction of crack growth. Obviously this assumption has limitations in the considered non-linear stress field and the investigation was limited to crack lengths equal to one quarter ($0.5b$) of the contact width ($2b$). For longer cracks FE methods must be used for calculations with the cracked geometry. Here the closed solutions (3) and (4) are taken.

Methods I and II

Two theories were used for the formation of cracks. The first (I) follows the widely accepted practice of assuming crack growth normal to the maximum principal stress in the crack opening mode with the stress intensity K_1, neglecting any influence of shear.

As the above may be a severe assumption in this case, a second theory (II) was used. This theory was proposed by Sih [13] and applied by Wojcik,[14] and includes all modes K_1, K_{11} (and K_{111} in 3-dimensional cases). It postulates crack growth in the direction of steepest decrease of the strain energy density (or local strain energy), which is given for plane strain by

$$\frac{dw}{dV} = \frac{(1+\nu)}{2E}\left[\sigma_x^2 + \sigma_y^2 - \nu(\sigma_x + \sigma_y)^2 + 2\tau_{xy}^2\right] \qquad (7)$$

Note: This criterion deviates slightly from the classical one that postulates that the crack growth is driven by the release of the total strain energy stored.

Both theories in linear fracture mechanics have been successfully used to predict the onset of rapid fracture if critical values are exceeded or to predict subcritical crack growth in fatigue, which was the aim of this study.

The following points are made regarding the application of these theories.

Remarks to Method I

The first theory (I) was used in a simplified form, following Bueckner [15] and Mariott,[16] allowing K_1 to be determined from the stress distribution in the uncracked body. The stresses existing in the uncracked body, which would be able to close the crack, were applied along the surface of the opened crack. However, the exact stress distribution was replaced by an approximation, which in the case of a crack starting at the surface (see Figure 6) can be written as

$$K_1 = 1.12\,(0.75\sigma_{av} + 0.25\sigma_{tip})\,\sqrt{(\pi a)} \qquad (8)$$

and was claimed by Mariott [16] to be within a few percent of extensive FE solutions. The calculations were done stepwise with a program allowing the starting point at the surface of a semi-infinite plane to be chosen along any point along the x-axis, and the crack growth was followed normal to the maximum principal stress σ_1, which in turn was numerically calculated from equations (3) and (4). The length a of the crack was taken as the secant of the curved crack path, σ_{av} and σ_{tip} determined and K_1 calculated with equation (8).

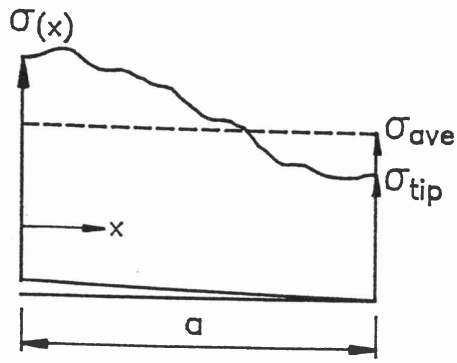

Figure 6. Averaging method of Mariott.[16]

The calculation was stopped when σ_{tip} became negative as the crack grew. This evidently would be different if the calculation was done with the cracked geometry and the length of the cracks shown in the results do not necessarily indicate the real length of the cracks. The tensile crack peak shown in Figure 5 would move downward to the tip of the crack and promote further crack growth.

Remarks to Method II

The second method establishes a strain energy density factor

$$S = r\frac{dW}{dV} \qquad (9)$$

which can reach a critical value S_c at which fracture will start. Under plane strain S can be related to K_1 and K_{11} by

$$S = a_{11}K_1^2 + a_{12}K_1K_{11} + a_{11}K_{11}^2$$

where the coefficients a_{11}, a_{12}, a_{22} are functions of the angle between the crack surface and the direction in which S is determined.

The critical value S_c and K_{1c} are related through

$$S_c = (1+\nu)(1-2\nu)\frac{K_{1c}^2}{2\pi E} \qquad (10)$$

A second method was used to determine S and then according to (10) an equivalent

$$K_{1e} = \frac{\sqrt{(2\pi)}ES}{(1+\nu)(1-2\nu)} \qquad (11)$$

was calculated, which can be directly compared to the K_1 obtained from the first method.

The second method starts from a point selected at the surface. It calculates the strain energy there and then searches on a half circle with radius r_0 for the direction of the steepest decrease of the strain energy density in which the crack is assumed to grow. The radius r_0 should be of the same order of magnitude as the thickness of the plastic zone. Growth of the crack was followed by increasing stepwise the radius around the same starting point and again determining the direction of the minimum strain energy density.

The cracks can run into regions of high hydrostatic pressure, depending on the starting point. Here the cracks will be subject to compression, and sliding of the crack surfaces on each other is impeded by friction and asperities.

Two load cases A and B

Load case A assumes the whole load to be repeating. The contact width was considered constant, so that the calculation does not present a rolling or sliding contact, but in the case of an external elliptic load, normal $p(x)$ (Figure 2) and tangential $fp(x)$ applied repeatedly. However this case did give some insight into the crack initiation in gears (Figure 1).

Load case B assumes the tangential load $fp(x)$ only to be repeating; the normal load $p(x)$ (Figure 2) was steady. This loading was similar to the T-head in Figure 3.

The criteria used at the crack tip to stop the crack growth calculation (although in practice the crack will not necessarily stop here) were:

For Method I:

Load case A	Stress normal to the crack $\sigma_n < 0$
Load case B	Steady plus repeating stress normal to the crack $\sigma_n < 0$

For Method II and both cases A and B:

If $\sigma_n < 0$ (compressive) and if the repeating shear stress across the crack faces $< f_c\sigma_n$.

Note that σ_n was always due to the steady plus the repeating load.

The coefficient of friction across the crack f_c was set $= 1$.

For both methods the crack growth direction and the stress intensity factor K_1 were calculated with repeating stresses only, assuming no influence of the steady stresses. Evidently these assumptions can be improved [15] to include the influence of hydrostatic pressure.

Results

The results are presented separately for the two load cases using both theoretical methods in each case.

Results load case A, whole load repeating

The calculations were done for starting points $x = 1.3-1.0$ (edge of contact at $x = 1.0$), $0.9-0.2$ and coefficients of friction $f = 0.1$ to 1.2. Crack paths were not found for all these parameters and of the existing ones only a selection at the edge of the contact area was shown.

Load case A method I (principal tensile stress promotes crack, K_1 from equation (8)) with a crack starting at the edge of the contact area $x = 1$ is shown in Figure 7. The same is done with method II (strain energy density method, tensile and shear stress promote crack K_{1e} from equation (11)) in Figure 8.

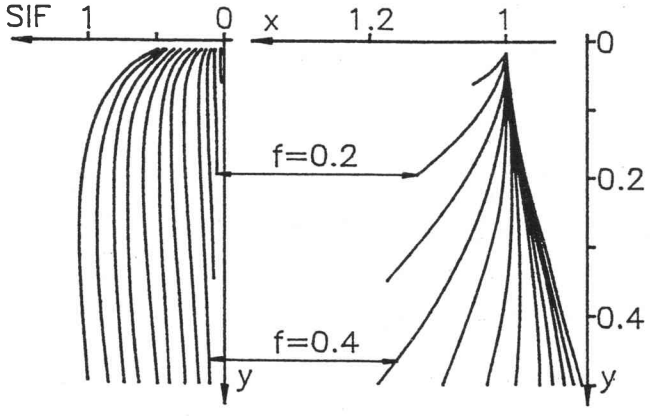

Figure 7. Load case A method I. Crack paths in the $x-y$ plane starting at the edge of the contact area at $x = 1$ and dimensionless stress intensity factors $SIF = K_1/\left(p_0\sqrt{b}\right)$ plotted over y. The coefficient of friction f varies from 0.1 to 1.2.

A comparison of the two methods shows some similarity of the crack paths and of the dimensionless stress intensity factors SIF and SIF_e. They reach a maximum and then decline (which may not happen when a calculation with a cracked geometry is carried out).

In order to find some understanding of the pitting formation in gears the neighbourhood of the left edge of the contact zone in Figure 2 was further investigated by varying the starting points of the crack. The coefficient of friction was kept in the range of $0.1-0.3$, as in gears 0.15 is the highest value to be expected. Figures 9 and 10 show a remarkable result, that cracks starting between $x = 0.9$

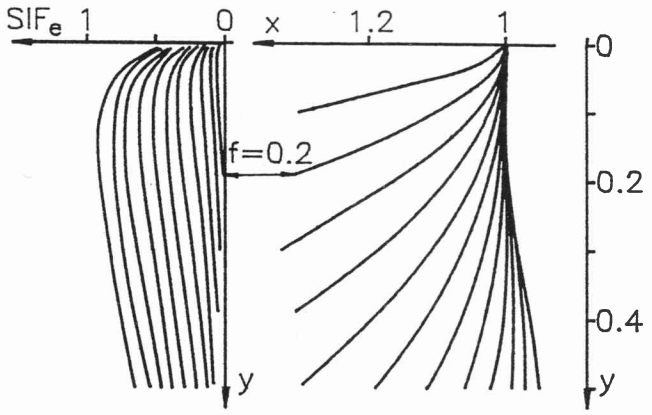

Figure 8. Load case A method II. Same plots as in Figure 7. However, $SIF_e = K_{1e}/\left(p_0\sqrt{b}\right)$ with K_{1e} from equation (11) was plotted over y.

and 1.3 line up to an asymtotic path irrespective of their starting point.

There are, however, differences between the results of the two methods. The angles of the asymptotes shown on the left side and the maximum SIF values for $f = 0.2$ are also slightly different. Beyond $x = 1.3$ the calculations were stopped as the stresses and SIF near the surface are small and the method II did not find solutions for small values of friction.

Discussion: load case A

Despite the differences between the two methods there seems to be reasonable agreement and cracks start in directions as observed in pitting (Figures 1 and 2). The crack path of method II for $f = 0.2$ in Figure 10 coincides with the 'valley' of $\tau_{\max} = 0$ (zero order) in the photoelastic test, on the left sides of Figure 4 (a) and (b). There is also a 'valley' of the strain energy density (Figure 11) into which the cracks run from different starting points, which explains why they all line up.

Most of the strain energy resides in or below the contact area and it is remarkable that only the small energy peak at $x = 1$ should produce a crack. Most conventional explanations for rolling damage point to the maximum shear stress $\tau_{\max} = 0.3p_0$ at $y = 0.78$, which certainly explains damage starting from defects at that lower y level. The two explanations, the conventional based on $\tau_{\max}$ and the one presented here, describe two distinct failure mechanisms, the first starting well below the surface and the second on the surface.

The angles of $12 - 32°$ on the left side of Figures 9 and 10 agree well with the angles $10 - 30°$ observed on gear teeth. Figure 12 from Joachim [18] shows such cracks below and above the pitch point. Steeper cracks only occur very close to the pitch point. The coefficient of friction is higher there.[1] Steeper cracks agree with crack paths shown in Figures 7 and 8.

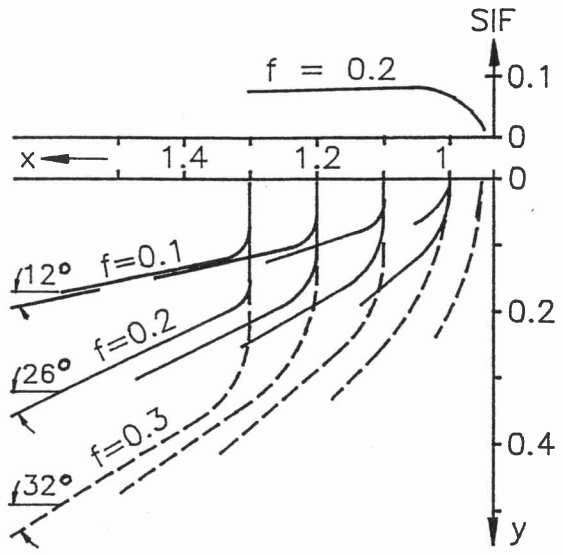

Figure 9. Load case A method I. Various crack paths with starting points near the left edge of the contact zone between $x = 0.9$ and 1.3 and maximum SIF values for $f = 0.2$. The coefficient of friction f varies from 0.1 to 0.3.

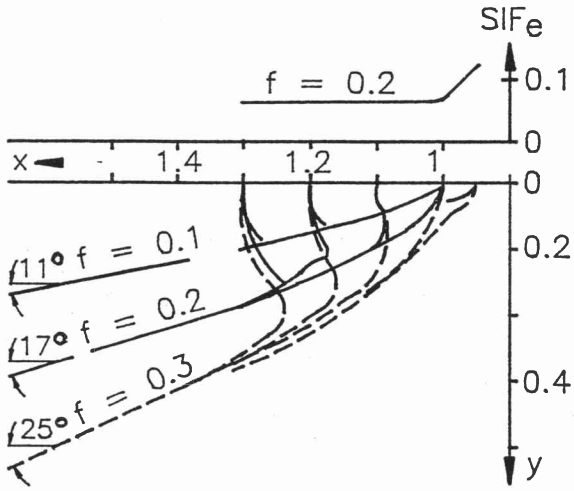

Figure 10. Load case A method II. Same plots as in Figure 7. However, SIF was replaced by SIF_e. The maximum of SIF_e (for $f = 0.2$) was approximately reached at $y_{\max} = 0.01$.

In sliding contacts, such as gears, the load in Figure 2 travels repeatedly over the surface and would be able to propagate cracks in the directions shown in Figures 9 and 10. The influence of such travelling loads on the growth of an existing crack could be calculated, but this was beyond the scope of this paper.

The dimensionless stress intensity factor SIF_e for $f = 0.15$ is approximately 0.035, which for example results with $p_0 = 1\,000$ MPa and $b = 0.2$ mm in

$$K_{1e} = SIF_e p_0\sqrt{b} = 0.35\ 10^9\sqrt{(0.0002)}Nm^{(-1.5)} = 5MNm^{(-1.5)} \quad (12)$$

This maximum K_{1e} value is reached at a crack depth (Figures 8 and 10) $y_{max}b = 0.024 * b = 4.8$ μm, but 50% of the maximum, i.e. $2.5MN\ m^{-1.5}$ is already reached at a depth of only 0.2 μm. As a comparison, the roughness and surface defects from which cracks can start of ground gears is $Ra = 0.25 - 0.5$ μm.

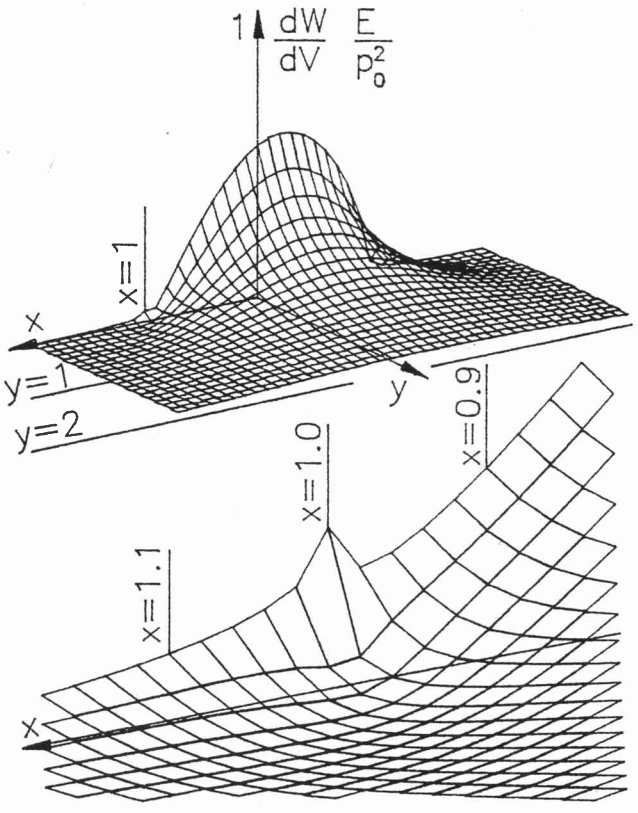

Figure 11. Load case A. Strain energy density in the contact zone. A close-up of the tiny energy peak at $x = 1$ is shown. A 'valley' in front of the peak can be seen.

K_{1e} in equation (12) is in the order of magnitude of the fatigue threshold value ΔK_{th} which in [4] is given as $6MN\ m^{-1.5}$, but other sources give lower values.

It could be concluded that the stress intensity found in these calculations is high enough to explain fatigue cracks starting in the direction as observed in gear teeth (Figure 2). Therefore the idea of cracks initiating on the left side of Figure 2 is confirmed.

There is another important aspect of the size effect. Equation (12) means that wider contact areas b, which in gears means larger modules, should use lower allowable Hertzian pressures p_0.

The crack at the right side of Figure 2 at $x = 1$ calculated with method I would not open and grow, as the normal stresses would be compressive (see Figure 5). Method II was not tried in this case, and Figure 11 also does not indicate the possibility of a crack starting at $x = 1$.

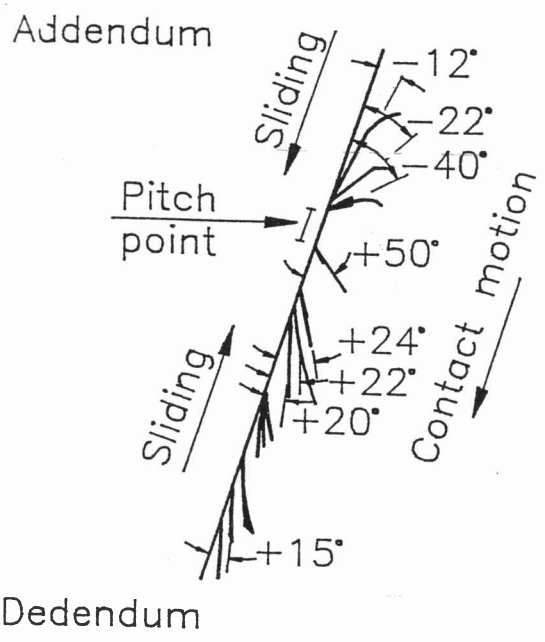

Figure 12. Cracks below and above the pitch point of a driven gear made of through hardened and tempered steel Ck 45 N.[16]

Results load case B, normal load steady, tangential load repeating

The calculations for load case B were done for similar parameters as in case A. Again crack paths were not found for all the parameters particularly with method II for cracks starting at $x > 1$.

Load case B method I with a crack starting at the edge of the contact area $x = 1$ is shown in Figure 13 and the same with method II in Figure 14.

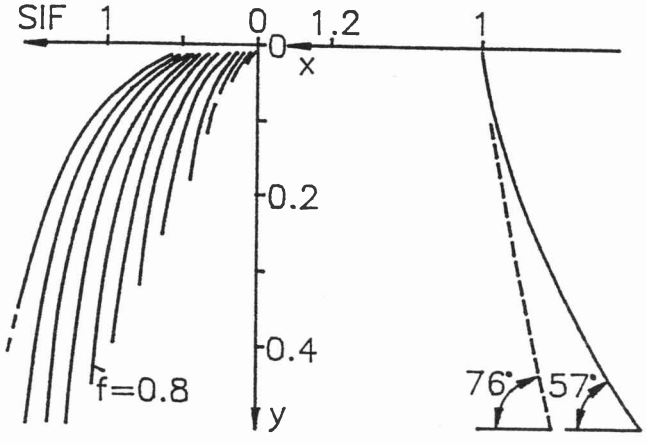

Figure 13. Load case B method I. Crack paths in the $x - y$ plane starting at the edge of the contact area at $x = 1$ and dimensionless stress intensity factors $SIF = K_1/(p_0\sqrt{b})$ plotted over y. The coefficient of friction f varies from 0.1 to 1.2, small values result in limited crack length. The dotted lines are for an additional repeating bending stress.

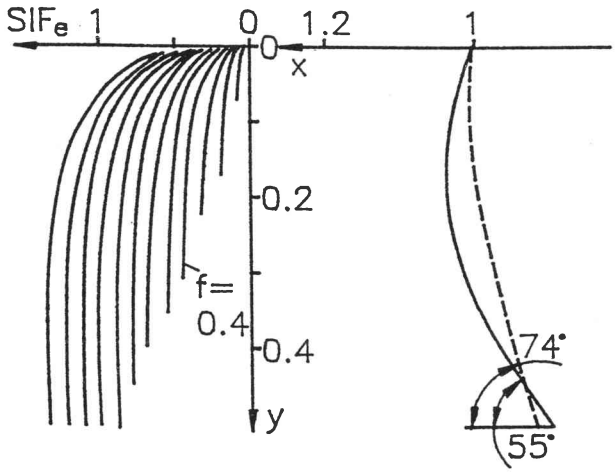

Figure 14. Load case B method II. Same plots as in Figure 13. However, $SIF_e = K_{1e}/\left(p_0\sqrt{b}\right)$ with K_{1e} from equation (11) was plotted over y.

In contrast to load case A there was no influence of the value of the coefficient of friction on the crack paths, although their length depends on the coefficient of friction. A comparison of the two methods again shows some similarity of the paths and of the dimensionless stress intensity factors SIF and SIF_e.

With the aim of finding some understanding of the crack formation in T-heads the neighbourhood of the left edge of the contact zone in Figure 3 was further investigated by varying the starting points of the crack. The SIF values are shown for $y = 0.05$ and $y = 0.4$ and a coefficient of friction $f = 0.8$, which is typical for highly loaded contacts [17;18] (Figures 15 and 16).

Figures 13 and 14 show that the crack calculation stopped at some limited crack length which increases with the coefficient of friction. Figures 15 and 16 show that inside the contact area ($x < 1$) cracks started only if the coefficient of friction was high enough. The minimum friction was 0.3 and for method II it went up to 0.5 for $x = 0.5$. Friction below this minimum was not able to start a crack.

In the T-head, repeated bending caused by the repeating horizontal force H (in Figure 3) is present in the left side of the contact. The right edge of the T-head at $x = 1$ is free of stresses whilst in the Hertzian case there are compressive stresses σ_x. The bending part of these stresses at $x = -1$ was approximated by a stress linear with y and added as a tensile repeating term to σ_x. The results at $x = 1$ are shown as dotted lines in Figures 13 and 14, and as dotted arrows in the SIF plots in Figures 15 and 16. The bending considerably increases the stress intensities, but hardly changes the crack paths.

Discussion: load case B

Agreement between the two methods was again quite good. Exceptions are the SIF values at $y = 0.4$ and the angles of the crack paths close to the loaded surface. This is due to the influence of shear (K_{II} mode) which is taken into account by method II. However, the angles at a distance $y = 0.5$ from the surface are generally less than $53 - 58°$ with small deviations. With the estimated influence of

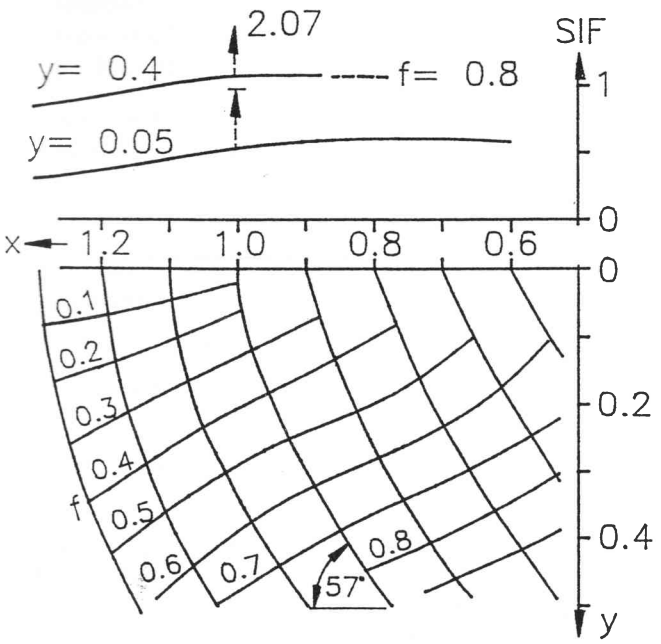

Figure 15. Load case B method I. Various crack paths with starting points between $x = 0.6$ and 1.3 and SIF values for $f = 0.8$ and $y = 0.1$ and $y = 0.4$. The coefficient of friction f on the left side and the associated lines indicate where the crack path calculation was stopped. For small f often no cracking was found.

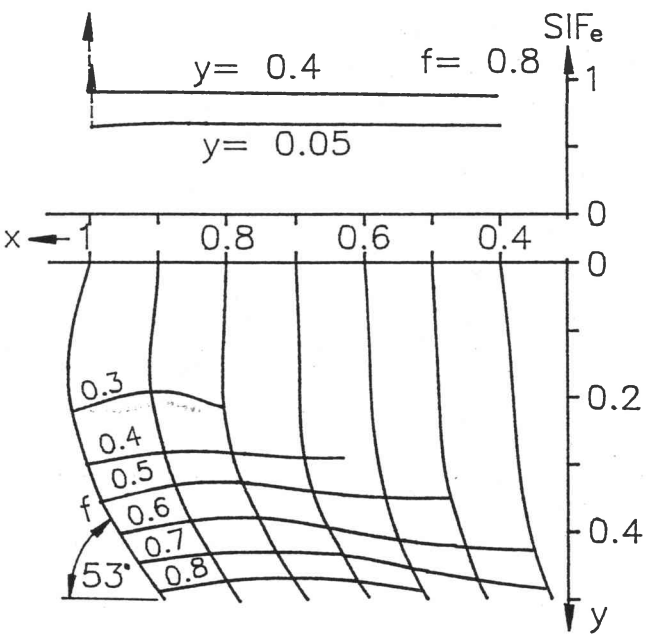

Figure 16. Load case B method II. Same plots as in Figure 14. However, SIF was replaced by SIF_e. The method II did not find solutions for $x > 1.01$.

bending the angles change to approximately 75° which is in good agreement with angles found in practice (Figure 3).

The dimensionless stress intensity factors SIF and SIF_e are not so different for both methods. However, both are roughly doubled by the superposition of bending, indicating that the Hertzian close field is strongly affected by the far field stresses in the tang of the T-head. The values of SIF and SIF_e show no prominent maximum at the edge $x = 1$ of the contact zone, suggesting that the crack should start there. However, the observed final cracks in Figure 3 show a preference for starting at $x = 1$. The mentioned step in the plastic zone may favour the crack location. Fretting may also create conditions which favour a crack location at the edge.

Ruiz et al. [20] and He & Ruiz [21] have run tests on dovetails and found that cracks started slightly inside the edge of the contact area near to the strongest fretting. The fretting was measured as an increase of roughness (Talysurf) to greater than 6 μm. The original machining roughness was 1 μm. The combined fatigue-fretting damage parameter ($FFDP$), defined as the product of the tangential σ_x stress, the shear stress and the relative sliding displacement controlled the crack growth where fretting played an important role.[19] The possibility of introducing the fretting roughness as starting crack length into the fracture mechanics was considered, but rejected due to the scarcity of experimental information.

The $FFDP$ parameter has the dimension N^2m^{-3} which is the square of the dimension of K. This means here again that in dovetails or in T-heads size effects are to be expected, demanding a reduction of pressure as the size b increases.

Conclusions

The two cases of fatigue cracking in gears and in T-heads can to a great extent be analysed by crack growth calculations starting from closed solutions. The directions of the crack paths agree well with those found in practice. In the case of gear cracks, the crack directions vary strongly with the coefficient of friction, whilst in the case of T-heads the crack direction is the same for all values of the coefficient of friction. Fatigue strength estimates based on initial defect sizes in gears are in the correct order of magnitude. Size effects make larger contact areas more susceptible to failure and require lower allowable pressures. The coefficient of friction is the governing parameter in all cases and should be kept as low as possible.

References

[1] Coutlakis J. *Contact stresses and crack mechanism in rolling/sliding contacts.* MSc thesis, University of Stellenbosch, 1990.

[2] Way S. Pitting due to rolling contact. *ASME Journal of Applied Mechanics*, 1935, **2**, pp.A49–A58.

[3] Bower AF. The influence of crack face friction and trapped fluid on surface initiated rolling contact fatigue cracks. *ASME Journal of Tribology*, 1988, **110**, pp.704–711.

[4] Kaneta M, Suetsugu M & Murakami Y. Mechanism of surface crack growth in lubricated rolling/sliding spherical contact. *ASME Journal of Applied Mechanics*, 1986, **53**, pp.354–360.

[5] Dudley D. *Gear Handbook. The design, manufacture and application of gears.* McGraw-Hill, 1962.

[6] Niemann G & Winter H. *Maschinenelemente.* Band 2, Springer-Verlag, 1985.

[7] Käser W. *Beitrag zur Grübchenbildung an gehärteten Zahnrädern.* Diss. T.U. München, 1984.

[8] Arcan M. Personal communication. Professor of Applied Mechanics, Tel Aviv University, Israel.

[9] King RN & Lindley TC. Fretting fatigue in a $3\frac{1}{2}$ NiCrMov rotor steel. *Advances in Fracture Research (FRACTURE 81)*, 1981, **2**, pp.631–640.

[10] Maul H. *Crack initiation by contact stresses.* BSc thesis, University of Stellenbosch, 1991.

[11] Föppl L. *Drang und Zwang.* Leibnitz Verlag, München, 1947.

[12] Smith JO & Liu CK. Stresses due to tangential and normal loads on an elastic solid with application to some contact stress problems. *ASME Journal of Applied Mechanics*, 1953, pp.157–166.

[13] Sih GC. *Mechanics of fracture initiation and propagation.* Kluwer Academic Publishers, Dordrecht/Boston/London, 1987.

[14] Wojcik R. Direction of crack growth initiation in roller contact: strain energy density criterion. *Theoretical and Applied Fracture Mechanics*, 1991, **15**(2), pp.191–198.

[15] Bueckner HF. A novel principle for the computation of stress intensity factors. *ZAMM*, 1970, **50**(9), pp.529–546.

[16] Mariott DL. *Beyond finite elements.* Seminar presented at University of Cape Town, 1991.

[17] Ellyin F. Cyclic strain energy density as a criterion for multiaxial failure fatigue. *EGF3*, Brown MW & Miller KJ (eds.). Mechanical Engineering Publications, London, 1989.

[18] Joachim FJ. *Untersuchungen zur Grübchenbildung an vergüteten und normalisierten Zahnrädern.* Diss. T.U. München, 1984.

[19] Hattori T, Sakata S & Ohnishi H. Slipping behavior and fretting fatigue in the disk/blade dovetail region. *IGTC 83 Tokyo*, 1983.

[20] Ruiz C, Boddington PHB & Chen KC. An investigation of fatigue and fretting in a dovetail joint. *Proceedings of the Society for Experimental Mechanics*, 1984, **XLI**, pp.208–217.

[21] He MJ & Ruiz C. Fatigue life of dovetail joints: verification of a simple biaxial model. *Proceedings of the Society for Experimental Mechanics*, 1989, **XLVI**, pp.126–131.